Available online at www.sciencedirect.com
SCIENCE DIRECT
Fluid Phase Equilibria 242 (2006) 43–56
FLUID PHASE EQUILIBRIA
www.elsevier.com/locate/fluid

Description of self-diffusion coefficients of gases, liquids and fluids at high pressure based on molecular simulation data

M.S. Zabaloy [a,*], V.R. Vasquez [b], E.A. Macedo [c]

[a] *Planta Piloto de Ingenieria Quimica, Universidad Nacional del Sur. CC 717, 8000 Bahia Blanca, Argentina*
[b] *Mail Stop 170, Chemical Engineering Department, University of Nevada-Reno, 1664N. Virginia St., Reno, NV 89557-0136, USA*
[c] *LSRE-Lab. Separation & Reaction Engineering, Departamento de Engenharia Química, Faculdade de Engenharia da Universidade do Porto-Rua do Dr. Roberto Frias, 4200-465 Porto, Portugal*

Received 1 June 2005; received in revised form 21 December 2005; accepted 22 December 2005
Available online 14 February 2006

Abstract

The purpose of this work is to evaluate the potential of modeling the self-diffusion coefficient (SDC) of real fluids in all fluid states based on Lennard–Jones analytical relationships involving the SDC, the temperature, the density and the pressure. For that, we generated an equation of state (EOS) that interrelates the self-diffusion coefficient, the temperature and the density of the Lennard–Jones (LJ) fluid. We fit the parameters of such LJ–SDC–EOS using recent wide ranging molecular simulation data for the LJ fluid. We also used in this work a LJ pressure–density–temperature EOS that we combined with the LJ–SDC–EOS to make possible the calculation of LJ–SDC values from given temperature and pressure. Both EOSs are written in terms of LJ dimensionless variables, which are defined in terms of the LJ parameters ε and σ. These parameters are meaningful at molecular level. By combining both EOSs, we generated LJ corresponding states charts which make possible to conclude that the LJ fluid captures the observed behavioral patterns of the self-diffusion coefficient of real fluids over a wide range of conditions. In this work, we also performed predictions of the SDC of real fluids in all fluid states. For that, we assumed that a given real fluid behaves as a Lennard–Jones fluid which exactly matches the experimental critical temperature T_c and the experimental critical pressure P_c of the real fluid. Such an assumption implies average true prediction errors of the order of 10% for vapors, light supercritical fluids, some dense supercritical fluids and some liquids. These results make possible to conclude that it is worthwhile to use the LJ fluid reference as a basis to model the self-diffusion coefficient of real fluids, over a wide range of conditions, without resorting to non-LJ correlations for the density–temperature–pressure relationship. The database considered here contains more than 1000 experimental data points. The database practical reduced temperature range is from 0.53 to 2.4, and the practical reduced pressure range is from 0 to 68.4.

Keywords: Dense fluids; Gases; Lennard–Jones; Molecular theory; Self-diffusion coefficient

1. Introduction

Self-diffusion is the diffusion of tagged particles of compound A in a fluid where all particles are chemically identical, i.e., where only compound A particles are present. Self-diffusion is characterized by the self-diffusion coefficient (SDC) D_{AA}, which relates the tagged A particle flux vector to the gradient of the partial mass density of tagged A particles [1]. On the other hand, the tracer (infinitely dilute) diffusion coefficient of component A (D_A^*) relates to the diffusion of labeled component A molecules within an homogeneous mixture [2] which may or may not contain untagged A molecules. In a binary homogeneous mixture of components A and B, where a small fraction of the A molecules are tagged, the tracer diffusion coefficient D_A^* tends to the self-diffusion coefficient D_{AA} [2] as the mole fraction of component A tends to unity. Coefficients D_{AA} and D_A^* correspond both to situations where the tagged particles are at infinite dilution, i.e., the system has no [tagged solute]–[tagged solute] interactions.

The more familiar mutual diffusion coefficient D_{AB} is important in process design calculations. For instance, it is required as input information for calculating mass transfer coefficients. The D_{AB} coefficient tends to the tracer diffusion coefficient D_A^*

* Corresponding author. Tel.: +54 291 486 1700x232; fax: +54 291 486 1600.
E-mail addresses: mzabaloy@plapiqui.edu.ar (M.S. Zabaloy), victor.vasquez@unr.edu (V.R. Vasquez), eamacedo@fe.up.pt (E.A. Macedo).

0378-3812/$ – see front matter © 2006 Elsevier B.V. All rights reserved.
doi:10.1016/j.fluid.2005.12.031

at the limit of infinite dilution of component A in component B. On the other hand, a model for the tracer diffusion coefficient D_A^* should match the condition $D_A^* = D_{AA}$ at the limit where the characteristic parameters of both components in the homogeneous mixture are forced to be identical [3]. At such limit, also the condition $D_{AB} = D_{AA}$ must be met.

This work is related to the need of modeling the self-diffusion coefficient of real fluids in wide ranges of temperature and pressure. The design of supercritical fluid extraction processes is a typical problem which implies a wide range of conditions.

Models based on molecular theory are those that make reference to parameters meaningful at molecular level. This is their distinguishing feature with respect to the so-called fully empirical models. Molecular theory ultimately provides analytical expressions for the dependency of thermodynamic and transport properties of model fluids on characteristic molecular level parameters and on variables such as temperature and density. By definition, model fluids are those for which the intermolecular potential function is known. Zabaloy et al. [4] provided more details.

The Lennard–Jones (LJ) fluid is suitable to be used as a reference for modeling properties of real fluids [4]. One of the LJ fluid important features is its realism. Ruckenstein and Liu (RL) [5] proposed a model for the self-diffusion coefficient of real fluids which is based on an expression for the self-diffusion coefficient of the LJ fluid as a function of temperature, density and LJ intermolecular potential parameters. In the RL model the density enters as input information into the expression for the self-diffusion coefficient. In cases where the experimental density was not available, Ruckenstein and Liu [5] used an empirical correlation for estimating it. Other LJ-based models for self-diffusion coefficient, such as that of Silva et al. [43] or the more recent model by Zhu et al. [6], are built in the same way, i.e., they require the density as input information. For pure compounds, the density is a function of temperature and pressure. The correlations for estimating the density from pressure and temperature can be of varying accuracy. On one hand, the simplest PVT equations of state (EOSs) can be used, e.g., the van der Waals EOS, which is known to have a poor performance for non-gas-like densities. At the other end of the spectrum, we find multi-parametric compound-specific EOSs which are very accurate, but require much experimental information on different properties, for every pure compound, to proceed to the (tedious) parameter fitting step. Even in the case of having available the coefficients of a multi-parametric PVT EOS for a large number of pure compounds of interest, the development of a LJ-based SDC model, such as the RL model, requires fitting parameters from experimental SDC information, due to the non-spherical nature of real fluid molecules. In spite of their accuracy, multi-parametric PVT EOSs are still empirical correlations, since their parameters are not meaningful at molecular level. The approach in this work is to combine a Lennard–Jones PVT EOS with a LJ SDC EOS. In this way, the calculation of the self-diffusion coefficient at given temperature and pressure is carried out by first calculating the LJ density, and then by calculating the self-diffusion coefficient from the previously computed LJ density. Hence, in this work, the density is used as an intermediate variable. Process modeling typically requires calculating properties at given pressure and temperature, rather than at given density and temperature. The purpose of this work is to establish whether the approach of combining PVT EOSs and SDC EOSs, of realistic model fluids, can be used as a basis for the development of real fluid SDC models, applicable over a wide range of conditions, thus removing the need for real fluid (compound-specific or not) PVT empirical correlations. Rather than proposing a polished model for the self-diffusion coefficient, we explore here the potential of an alternative modeling approach.

2. Model fluids

Well-known model fluids are for instance the hard spheres fluid, the square well fluid and the Lennard–Jones [LJ] fluid. Only repulsive interactions are present in the hard spheres fluid. Therefore, it does not exhibit a vapor–liquid phase transition [1]. On the other hand the Lennard–Jones fluid shows vapor–liquid, solid–liquid and solid–vapor transitions, a critical point and a triple point. A phase diagram of the LJ fluid is available in, e.g., reference [4]. The expression for the Lennard–Jones intermolecular potential is the following.

$$u(r) = 4\varepsilon \left[\left(\frac{\sigma}{r}\right)^{12} - \left(\frac{\sigma}{r}\right)^{6} \right] \tag{1}$$

where r is the intermolecular distance, u the potential energy, ε the depth of the LJ potential well and σ is the LJ separation distance at zero energy. Because the parameters ε and σ are clearly defined features of the LJ intermolecular potential function, we can assert that, within the universe of the LJ fluid, the parameters ε and σ are meaningful on the molecular level.

The LJ reduced temperature T^+, reduced pressure P^+, reduced density ρ^+, and reduced self-diffusion coefficient D^+ are conventionally defined as follows:

$$T^+ = \frac{kT}{\varepsilon} \tag{2}$$

$$P^+ = \frac{P\sigma^3}{\varepsilon} \tag{3}$$

$$\rho^+ = \frac{N}{V}\sigma^3 = N_A \rho \sigma^3 \tag{4}$$

$$D^+ = D\frac{\sqrt{m/\varepsilon}}{\sigma} \tag{5}$$

where k is the Boltzmann constant, T the absolute temperature, P the absolute pressure, N the number of molecules, V the system volume, N_A the Avogadro's number, ρ the amount-of-substance density in units such as mole per liter, D the self-diffusion coefficient and m is the mass of one molecule. The variable ρ^+ for the LJ substance in fluid state is not necessarily limited to values less than unity.

3. Self-diffusion coefficient for the Lennard–Jones fluid

Rowley and Painter (RP) [7] computed LJ self-diffusion coefficients at 171 different conditions using the method of molecular

dynamics. Rowley and Painter [7] covered a wide range of temperature ($0.8 \le T^+ \le 4$) and density. The range for ρ^+ [7] was from zero to the minimum between 1 (unity) and the density of the dense LJ fluid at equilibrium with the LJ solid ($\rho^+_{\text{fluid,SFE}}$). More recently Meier et al. [1,42] computed, among other properties, the self-diffusion coefficient for the Lennard–Jones model fluid, at 334 different temperature–density conditions, from equilibrium molecular dynamics simulations, covering the entire fluid region from the low density gas to the compressed fluid close to the freezing line. Meier et al. [1,42] LJ self-diffusion coefficient data correspond to the reduced temperature range from $T^+ = 0.7$, which is close to the LJ triple point temperature, to $T^+ = 6$, which is about 4.5 times the critical temperature. Meier et al. [1,42] LJ self-diffusion data are distributed among 16 different isotherms. Meier et al. [1,42] used a larger number of particles, larger cutoff radii and much longer simulation runs than considered before in conventional simulation work, and demonstrated that his simulation data for the LJ transport coefficients are significantly more accurate than in previous studies. The estimated uncertainty of Meier et al. data is about 0.5–1%.

Rowley and Painter [7] correlated their LJ self-diffusion coefficient data using the following equation:

$$D^+\rho^+ = (D^+\rho^+)_0 + \sum_{i=1}^{4}\sum_{j=1}^{6} b_{ji}\frac{(\rho^+)^i}{(T^+)^{(j-1)}} \tag{6}$$

where $(D^+\rho^+)_0$ is the limit of the product $(D^+\rho^+)$ as the density approaches zero and the coefficients b_{ji} are general LJ fitting parameters. The self-diffusion coefficient D^+ tends to infinity at the zero density limit [1]. On the other hand, at the zero density limit, the product $(D^+\rho^+)$ remains finite and takes the values known from the Chapman–Enskog solution to the Boltzmann equation [1]. The product $(D^+\rho^+)_0$ depends only on the temperature T^+.

In this work we did not use the values that Rowley and Painter [7] reported for the coefficients b_{ji}. Rather, we computed new values for the coefficients b_{ji} by forcing a good reproduction of Meier's [1,42] LJ self-diffusion data, which cover temperature and density ranges wider than those of Rowley and Painter [7]. For the term $(D^+\rho^+)_0$ we used Eq. (B.1) of page 193 of Meier's [1] Ph.D. thesis, which, rewritten in terms of dimensionless variables, becomes Eq. (A.1) of Appendix A. Eq. (A.1) has an extremely wide range of applicability: from $T^+ = 0.7$ to 1000; and is written in terms of a number of collision integrals for the Lennard–Jones fluid (see Appendix A). We report the values obtained in this work for the b_{ji} coefficients in Table 1.

The range of applicability of Eq. (6) coupled to Table 1 parameters is the same than that of Meier et al. [1,42] LJ self-diffusion coefficient data, i.e., for the density, from zero to $\rho^+_{\text{fluid,SFE}}$ ($\rho^+_{\text{fluid,SFE}}$ = density of the dense LJ fluid in equilibrium with the LJ solid), and, for the temperature, from $T^+ = 0.7$ to 6. The density $\rho^+_{\text{fluid,SFE}}$ is a function of only T^+. Zabaloy et al. [4] presented an iterative procedure to compute $\rho^+_{\text{fluid,SFE}}$. In view of the T^+ range of applicability of Eq. (6) we propose here to calculate $\rho^+_{\text{fluid,SFE}}$ using the following simple equation:

Table 1
Values for the parameters of Eq. (6) obtained in this work

j	i	b_{ji}	j	i	b_{ji}
1	1	−0.840222	1	3	−1.078374
2	1	3.073654	2	3	1.666815
3	1	−3.991659	3	3	0.698998
4	1	2.018800	4	3	−6.050100
5	1	−0.523600	5	3	3.520100
6	1	0.104100	6	3	−0.247500
1	2	0.958776	1	4	0.346849
2	2	−2.833311	2	4	−0.168102
3	2	0.206392	3	4	−0.059826
4	2	6.207900	4	4	1.089544
5	2	−4.590900	5	4	−0.135200
6	2	0.805200	6	4	−0.303090

$$\rho^+_{\text{fluid,SFE}} = 0.92146891(T^+)^{0.21839684} \tag{7}$$

which reproduces well the data of Agrawal and Kofke [8] for the density of the dense LJ fluid at solid–fluid coexistence in the temperature range from the LJ triple point T^+ up to $T^+ = 10$. Eq. (6) coupled to Table 1 parameters gives, for the Meier et al. [1,42] set of 334 LJ self-diffusion coefficient data, an average absolute value relative deviation of 0.68% with a maximum deviation of 3.24%. The bias is 0.045%. The absolute value of the coefficients in Table 1 is in all cases less than 7. On the other hand, some coefficients in reference [7] have absolute values in the order of 400. We used the following procedure to find initial estimates of the parameters of Eq. (6). For a given isothermal LJ self-diffusion data subset, i.e., at a given constant T^+, we fitted the residual property $\left\lfloor D^+\rho^+ - (D^+\rho^+)_0 \right\rfloor$ as a fourth order polynomial function of ρ^+ with zero intercept, in agreement with Eq. (6). We repeated this task for the 16 Meier et al. isothermal data sets. Then, for every power of ρ^+, i.e., for powers from 1 to 4, we correlated the 16 coefficients found previously, as a 5th order polynomial function of the variable $1/T^+$. In this way we obtained excellent initial estimates for the 24 b_{ji} coefficients of Eq. (6). Then, we readjusted them all simultaneously but found almost no difference between the initial set and the optimum set.

Eq. (6) coupled to the parameter values of Table 1 makes possible the analytical fast computation of self-diffusion coefficients for the Lennard–Jones fluid over a wide range of conditions from known values of T^+ and ρ^+. Eq. (6) should not be used outside the established temperature and density ranges.

According to Lee and Thodos [9] and De et al. [10], the properly interpreted experimental evidence implies that no anomaly in the vicinity of the critical point exists for the self-diffusion coefficient of real fluids. For the self-diffusion coefficient of the LJ fluid, Meier [1] did not report any critical anomaly either. Consistently, Eq. (6) does not account for any critical enhancement effect.

Fig. 1 illustrates the representation of part of the Meier et al. [1,42] LJ SDC data by Eq. (6). The product $(D^+\rho^+)$ is plotted as a function of ρ^+ at different values of T^+. The $T^+ = 0.7$

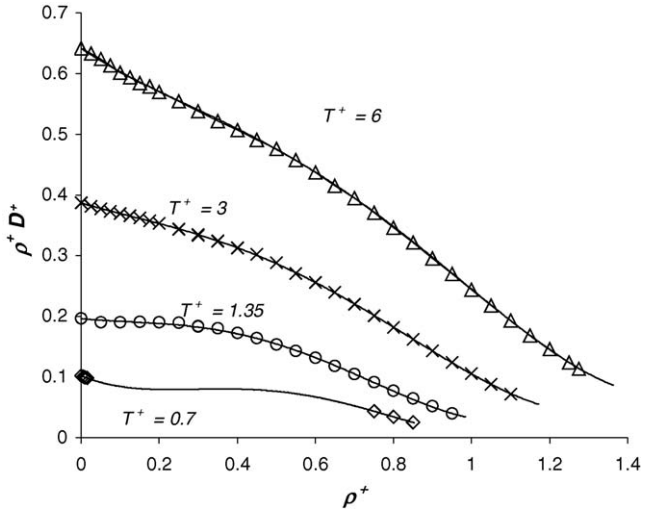

Fig. 1. Product $(D^+\rho^+)$ for the Lennard–Jones fluid as a function of the density ρ^+ at varying temperature T^+ values. Symbols (△, ×, ◯, ◊) denotes molecular dynamics results [1,42]. Solid lines: Eq. (6)/Table 1.

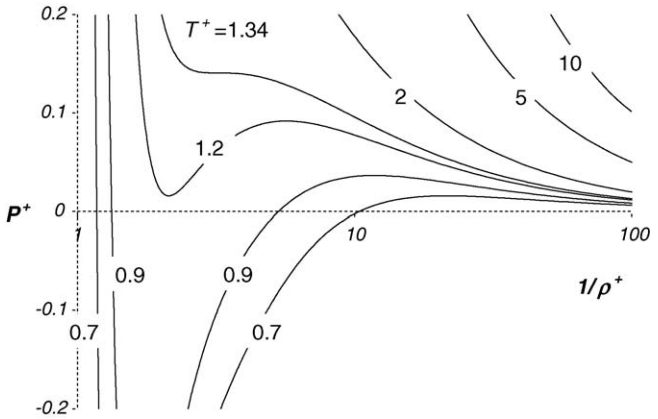

Fig. 2. Pressure as a function of reduced molar volume $(1/\rho^+)$ for the Lennard–Jones fluid at subcritical and supercritical temperatures. We generated the curves using Eq. (8).

isotherm is close to the triple point isotherm. At such temperature, the density interval without SDC data is relatively wide and corresponds to the two-phase region. In spite of this, Eq. (6) does not show, for such interval, problematic loops, i.e., Eq. (6) properly interpolates LJ liquid and vapor SDC information. The three higher temperature isotherms in Fig. 1 correspond to supercritical isotherms.

4. Lennard–Jones pressure–density–temperature equation

The independent variables in Eq. (6) are the temperature and the density. However, from the process design point of view the pressure is an independent variable more convenient than the density. Hence we need a PVT equation of state for the LJ fluid to make possible the computation of density from known values of temperature and pressure. The PVE/hBH LJ-EOS, developed by Kolafa and Nezbeda [11], is an accurate LJ PVT EOS which is based on critically assessed computer simulation data from several sources. According to Ref. [11], the PVE/hBH LJ-EOS has an accuracy comparable with or better than that of LJ PVT EOSs previously available, such as those of Johnson et al. [44] or Nicolas et al. [45], particularly with regard to the critical point as shown in Fig. 11 of Ref. [11]. The PVE/hBH LJ-EOS [11] is the LJ PVT EOS we use in this work and it is the following:

$$z = \frac{P^+}{\rho^+ T^+} = f_{\mathrm{KN}}(\rho^+, T^+) \tag{8}$$

where z is the compressibility factor and f_{KN} is a function of ρ^+ and T^+. The function f_{KN} is available in the original reference [11] and more concisely in reference [4]. The temperature range of applicability of Eq. (8) is $0.68 \leq T^+ \leq 10$. The range for ρ^+ is from 0 (zero) to the density of the dense LJ fluid in equilibrium with the LJ solid $(\rho^+_{\mathrm{fluid,SFE}})$ (see Eq. (7)). Notice that the range of applicability of Eq. (8) completely contains that of Eq. (6). Eq. (8) does not account for any special phenomena in the critical region, i.e., it is a classical LJ PVT EOS. The critical coordinates corresponding to Eq. (8) are the following [11]:

$$T_{\mathrm{c}}^+ = 1.3396 \tag{9}$$

$$P_{\mathrm{c}}^+ = 0.1405 \tag{10}$$

$$\rho_{\mathrm{c}}^+ = 0.3108 \tag{11}$$

$$z_{\mathrm{c}} = 0.3375 \tag{12}$$

Fig. 2 shows the pressure P^+ as a function of the inverse density ρ^+ for several isotherms. All curves correspond to Eq. (8). The variable $1/\rho^+$ is a reduced molar volume. The subcritical isotherms have pressure regions where, at a given set pressure, there are two meaningful values of density (vapor and liquid). The critical isotherm shows a characteristic flat region where the volume is very sensitive to small changes in pressure. At supercritical temperatures there is only one density value compatible with a set pressure value.

The user should make sure that Eqs. (6) and (8) are used within the proper density range by using Eq. (7) to compute the maximum density of applicability.

In summary, the equations we presented up to this point make it possible to analytically and quickly calculate the LJ SDC D^+ at a given temperature T^+ and pressure P^+ within proper temperature and density ranges. Such equations interpolate and smooth LJ thermodynamic and transport data obtained through typically long molecular simulation runs.

5. Corresponding states LJ charts involving the self-diffusion coefficient

Eqs. (6) and (8) interrelate sets of dimensionless variables. This indicates that the Lennard–Jones fluid is a corresponding states model fluid, whose dimensionless variables are defined in terms of parameters meaningful at molecular level, namely ε and σ.

Fig. 3 shows the product $(D^+\rho^+)$ as a function of pressure P^+ at varying values of temperature T^+. We generated Fig. 3 by combining Eqs. (6) and (8), i.e., at chosen values of T^+ and ρ^+,

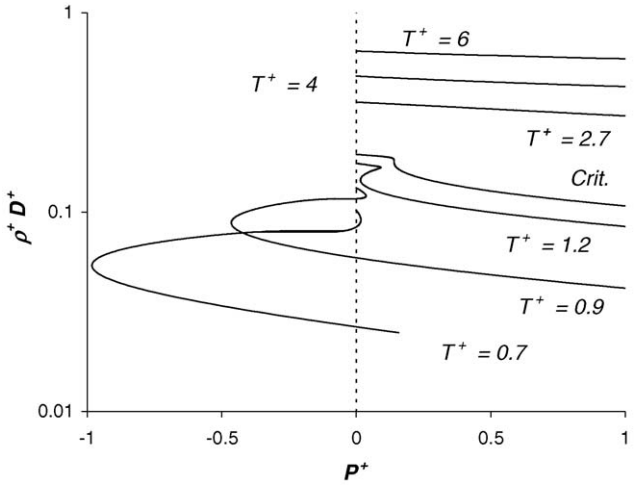

Fig. 3. Product $(D^+\rho^+)$ for the Lennard–Jones Fluid as a function of the pressure P^+ at varying temperature T^+ values, as represented by Eqs. (6) and (8).

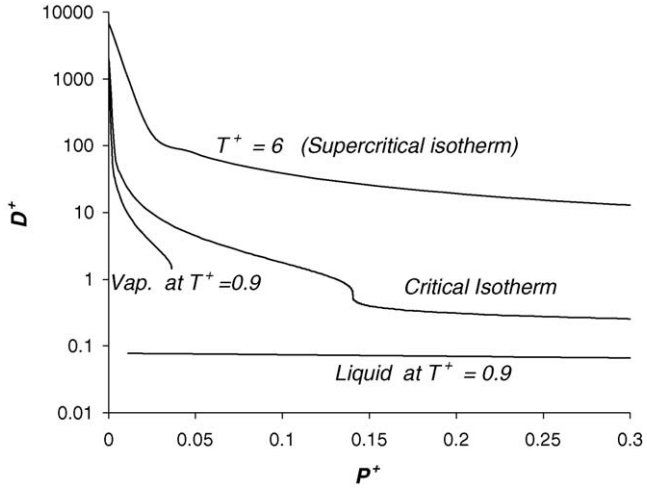

Fig. 4. Self-diffusion coefficient D^+ for the Lennard–Jones Fluid as a function of the pressure P^+ at varying temperature T^+ values, as represented by Eqs. (6) and (8).

we computed the product $(D^+\rho^+)$ and the pressure P^+, respectively, from Eqs. (6) and (8) and plotted the result. For a given isotherm the computations are performed from zero density up to a high enough density (which is at most equal to $\rho^+_{\text{fluid,SFE}}$). The plot shows three subcritical isotherms, the critical isotherm and three supercritical isotherms. The zero pressure starting point for all isotherms corresponds to the Chapman–Enskog zero density value for the product $(D^+\rho^+)$. The loops for the three subcritical isotherms are the result of van der Waals loops associated to Eq. (8). For the $T^+ = 0.7$ and 0.9 (subcritical) isotherms the loops include regions of unphysical negative pressure. This does not constitute a problem since the pressure is always the set degree of freedom in practical calculations, and it is always set as a positive variable. The critical isotherm shows a steep region where small changes in pressure produce important changes in the product $(D^+\rho^+)$. At high temperature the product $(D^+\rho^+)$ is less sensitive to pressure. For given temperature and phase type (vapor, liquid or supercritical fluid), the product $(D^+\rho^+)$ appears to be a monotonically decreasing function of pressure. For any of the three subcritical isotherms, the pressure P^+, seen as a function of the product $(D^+\rho^+)$ in Fig. 3, shows a local maximum and a local minimum. The portion of the curve between the two extrema corresponds to the density range where the LJ PVT EOS, i.e., Eq. (8), violates the mechanical stability criterion. Such portion of the curve is thus meaningless. The behavior of the LJ product $(D^+\rho^+)$ is simpler than that of the LJ viscosity [4].

Fig. 4 shows, for the LJ fluid, the diffusion coefficient D^+ as a function of the pressure P^+ at different values of the temperature T^+. We generated Fig. 4, again by using Eqs. (6) and (8) at set values of T^+ and ρ^+, but solving in this case Eq. (6) for D^+. This last step implied set values of ρ^+ which had to differ from zero (notice the logarithmic scale in Fig. 4). The maximum P^+ value in Fig. 4 corresponds roughly to twice the critical pressure. For the subcritical isotherm at $T^+ = 0.9$ we removed all points with negative pressure P^+ and/or all points with negative derivative of P^+ with respect to ρ^+. For such isotherm there is a range of P^+ values within which we find both, a vapor-like and a liquid-like value of D^+. Only one of such P^+ values corresponds to a situation of vapor–liquid equilibrium. All other P^+ values within the vapor–liquid P^+ range correspond to a metastable condition either for the vapor phase or for the liquid phase. Fig. 4 depicts the SDC behavior typically found in real fluids, i.e., (a) at given temperature and pressure, a vapor has a SDC greater than that of a liquid, (b) the SDC decreases with pressure and increases with temperature and (c) the critical isotherm shows a large sensitivity of the SDC with respect to pressure around the critical pressure. Fig. 4 shows that equations Eqs. (6) and (8) can basically represent the self-diffusion coefficient of subcritical vapors and liquids, and of near-critical or (light or dense) supercritical fluids in wide pressure ranges.

It is useful to have available Lennard–Jones corresponding states charts in terms of practical reduced properties. These are more familiar to the engineering community than the LJ reduced properties of Eqs. (2)–(5). To that end, we introduce the equations that follow.

For a Lennard–Jones fluid, it can be shown, from Eq. (2), that

$$T^+ = T_r T_c^+ \tag{13}$$

where T_c^+ is a constant [Eq. (9)] and T_r is the practical reduced temperature, defined as:

$$T_r = \frac{T}{T_c} \tag{14}$$

where T_c is the critical temperature. A chosen value of T_r sets a value for T^+ through Eq. (13). Also, from Eq. (3), we write

$$P^+ = P_r P_c^+ \tag{15}$$

where P_c^+ is a constant [Eq. (10)] and P_r is the practical reduced pressure, defined as:

$$P_r = \frac{P}{P_c} \tag{16}$$

where P_c is the critical pressure. A chosen value of P_r sets a value for P^+ through Eq. (15). On the other hand, for the LJ

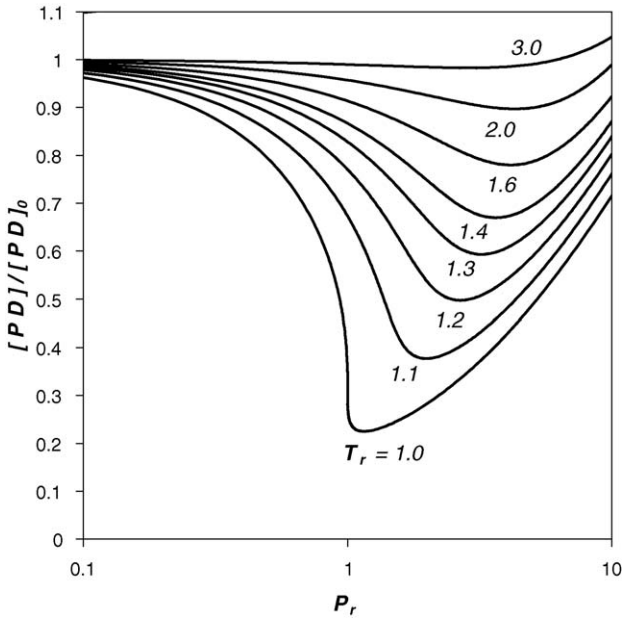

Fig. 5. Ratio PD/(PD)$_{P\to 0}$ as a function of the P_r at different values of T_r for the Lennard–Jones fluid.

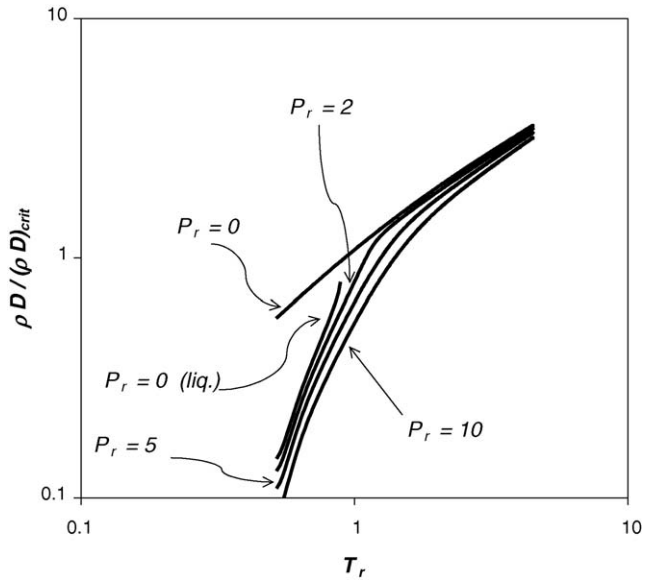

Fig. 6. Practical reduced self-diffusion coefficient density product as a function of the practical reduced temperature T_r for different isobars (constant P_r) for the Lennard–Jones fluid.

fluid, it can be shown that

$$\frac{\mathrm{PD}}{(\mathrm{PD})_{P\to 0}} = \frac{P^+}{\rho^+ T^+}\frac{D^+\rho^+}{(D^+\rho^+)_0} \tag{17}$$

where PD is the product of pressure times the self-diffusion coefficient at a given temperature, while (PD)$_{P\to 0}$ is the limit of PD as pressure tends to zero. To derive Eq. (17) it is necessary to remember that Eq. (8) matches the ideal gas law, i.e., as ρ^+ tends to zero the pressure P^+ tends to the product $[\rho^+T^+]$. Fig. 5, shows the quotient PD/(PD)$_{P\to 0}$ as a function of P_r at different values of T_r for the LJ fluid. A given point is generated as follows: set a value of T_r. Calculate T^+ through Eq. (13). Calculate $(D^+\rho^+)_0$ from Eq. (A.1). Set a value of ρ^+ less than or equal to $\rho^+_{\mathrm{fluid,SFE}}$ [Eq. (7)] and calculate the product $(D^+\rho^+)$ using Eq. (6), P^+ using Eq. (8) and P_r using Eq. (15). Calculate the ratio PD/(PD)$_{P\to 0}$ using Eq. (17). Fig. 5 is quite similar to Fig. 16.3-1 of Bird et al. [12], which is based on theory and on some (very few) fragmentary data.

The practical reduced self-diffusion coefficient density product $(D\rho)_r$ is defined as:

$$(D\rho)_r = \frac{(D\rho)}{(D\rho)_{\mathrm{crit}}} \tag{18}$$

where $(D\rho)_{\mathrm{crit}}$ is the product $D\rho$ at the critical point. On the other hand, the product $(D^+\rho^+)$, evaluated using Eq. (6)/Table 1, at the temperature and density conditions of Eqs. (9) and (11) is the following:

$$(D^+\rho^+)_{\mathrm{crit}} = 0.179961 \tag{19}$$

Notice that for the LJ fluid

$$(D\rho)_r = \frac{(D^+\rho^+)}{(D^+\rho^+)_{\mathrm{crit}}} \tag{20}$$

The reduced product $(D\rho)_r$ can be calculated at given P_r and T_r, as follows: calculate P^+ from Eq. (15). Compute T^+ from Eq. (13), ρ^+ from Eq. (8), $(D^+\rho^+)$ from Eq. (6)/Table 1, and $(D\rho)_r$ from Eqs. (19) and (20). Since Eq. (8) can give one or two meaningful values of ρ^+, this calculation procedure can give one or two values for $(D\rho)_r$. Using this procedure we generated Fig. 6, which shows the practical reduced SDC density product as a function of the practical reduced temperature T_r for different isobars for the Lennard–Jones fluid. The curve labeled "$P_r = 0$" is the zero density limit, while the curve identified as "$P_r = 0$ (liquid)" corresponds to the liquid-like root which Eq. (8) gives at zero pressure for certain temperature range. Fig. 6 is in good agreement with Fig. 17.2-1 of page 522 of Ref. [13] which was generated from a combination of theory and real fluid experimental data. On the other hand, Fig. 6 is based only on molecular simulation data.

From the information we presented in this section, we conclude that the Lennard–Jones fluid, as represented by the combined LJ self-diffusion coefficient (SDC) equation of state [Eq. (6)] and by the LJ pressure–density–temperature EOS [Eq. (8)], has a behavior, over a wide range of conditions, consistent with that observed for real fluids.

6. Prediction of self-diffusion coefficients of real fluids based on Lennard–Jones molecular simulation data

In this section we study how the analytical expressions for the pressure and the self-diffusion coefficient for the Lennard–Jones fluid, i.e., the combined Eqs. (6) and (8), perform when predicting the SDC of real fluids. To that end, we need to assign numerical values to the LJ parameters ε and σ. Fig. 4 shows the important differences in the patterns which the self-diffusion coefficient follows, depending on the location of the temperature and pressure conditions with respect to those of the critical

Table 2
Sample self-diffusion coefficient prediction for methane at 160 K and 16.49 bar

Input data

Compound	M_w (g mol^{-1}) [14]	T_c (K) [14]	P_c (bar) [14]	T (K)	P (bar)
Methane	16.0428	190.564	45.99	160	16.49

Calculated variables

ε/κ (K) [Eq. (21)]	σ (Å) [Eq. (22)]	T^+ [Eq. (2)]	$\rho^+_{fluid,SFE}$ at T^+ [Eq. (7)]	$(D^+\rho^+)_0$ [Eq. (A.1)]	P^+ [Eq. (3)]
142.3	3.91	1.12474549	0.94543304	0.1650568	0.05037715

Phase A

Type	ρ^+_A [Eq. (8)]	$(D^+\rho^+)_A$ [Eq. (6)]	D_A (m^2/s) [Eq. (5)]	Experimental D_A (m^2/s) [36]
LIQ	0.62251642	0.10742399	1.83×10^{-8}, prediction error: +5%	1.75×10^{-8}

Phase B

Type	ρ^+_B [Eq. (8)]	$(D^+\rho^+)_B$ [Eq. (6)]	D_B (m^2/s) [Eq. (5)]
VAP	0.05957616	0.15998618	28.54×10^{-8}

point. From Fig. 4, it seems reasonable to treat a given real fluid as a LJ fluid having critical temperature and pressure coordinates identical to the experimental critical temperature and the experimental critical pressure, respectively. To impose such full consistency with the experimental critical temperature and pressure we combine Eqs. (2), (3), (9) and (10) to give:

$$\varepsilon = \frac{\kappa T_c}{T_c^+} = \frac{\kappa T_c}{1.3396} \tag{21}$$

$$\sigma = \left(\frac{\kappa T_c}{P_c}\frac{P_c^+}{T_c^+}\right)^{1/3} = \left(\frac{\kappa T_c}{P_c}\frac{0.1405}{1.3396}\right)^{1/3} \tag{22}$$

If, for a given real fluid, we compute parameter ε from the experimental critical temperature T_c through Eq. (21), and parameter σ from T_c and from the experimental critical pressure P_c through Eq. (22), then, the resulting Lennard–Jones fluid will have its critical state at the same T, P coordinates than the real fluid. In view of the non-Lennard–Jones nature of real fluids, the ε and σ parameters computed as described should be considered as effective LJ parameters.

The only input experimental information we use in this work, when calculating the SDC for a real fluid at given temperature and pressure, is the critical temperature T_c, the critical pressure P_c and the molecular weight M_w. We used the values of T_c, P_c and M_w available in Ref. [14], for all real fluids here considered. Table 2 provides a numerical calculation example that illustrates the use of the above equations. The example consists of predicting, from T_c, P_c and M_w, the self-diffusion coefficient of methane at 160 K and 16.49 bar. At the set T and P values in the example, Eq. (8) provides two meaningful density values, and hence we come out with two SDC values (liquid-like and vapor-like). Notice that, on one hand, none of the two density values exceeds the LJ fluid density at solid fluid equilibrium ($\rho^+_{fluid,SFE}$), while; on the other hand, the T^+ value falls within the applicability ranges of Eqs. (6) and (8). When carrying out calculations using a large real fluid SDC database for assessing the prediction performance of the model, we found that some real fluid SDC experimental data, available in the literature, corresponded to conditions falling outside the applicability ranges of Eqs. (6) and (8). We do not report results here for such situations, which imply the need for extrapolation schemes applicable to the Lennard–Jones SDC and PVT equations of state here considered.

The calculation procedure described in Table 2 corresponds to the relatively crude model which, as a case study, we used in this work to assess the potential of our alternative modeling approach. We computed the density values in Table 2 using Eq. (8). Thus, such values are Lennard–Jones densities which may differ from the experimental methane densities.

If a user wanted to compute the self-diffusion coefficient for a given pure compound using the procedure of Table 2, at set values of temperature and density (instead of temperature and pressure), he/she would first need to find the pressure from the set density and temperature values, using a reliable PVT model for the given pure compound (or a table of experimental PVT values), and then follow the procedure of Table 2. A by product of the application of such procedure would be a Lennard–Jones density value that in general will differ from the set density value.

7. Results and discussion

For a few real compounds, we begin this section by illustrating graphically the performance of the predictive Lennard–Jones-based model for the self-diffusion coefficient.

Fig. 7 shows experimental and predicted self-diffusion coefficient values, as a function of pressure, for Krypton, at two different temperature values, both greater than Krypton's T_c. The circles represent the experimental data at 293 K. The experimental data with the label "220.4 K" (triangles) actually correspond to a few temperature values with a relatively narrow range of variation (standard deviation: 0.9 K). The solid lines represent the model predictions we made from T_c, P_c and M_w. The pressure reaches relatively high values (greater than 50 bar). We see

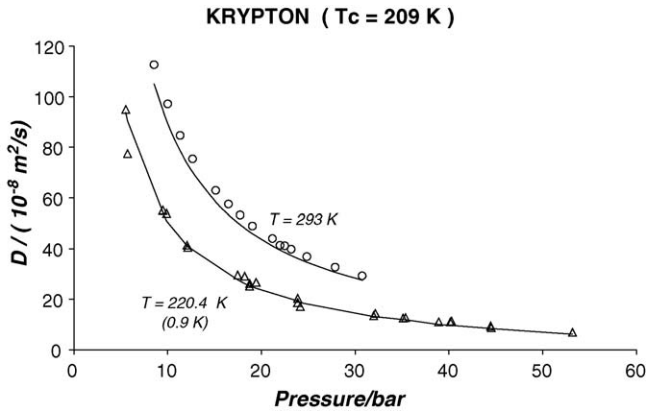

Fig. 7. Self-diffusion coefficient (SDC) as a function of pressure for Krypton. The solid lines correspond to model predictions. Experimental data: △ [19], ◯ [21]. The experimental data presented for the 220.4 K isotherm (△) actually correspond to a range of temperature values (standard deviation: 0.9 K).

that the model properly follows the experimental data. Eq. (1) implies that the Lennard–Jones fluid is made of spherical (i.e., simple) molecules which can attract or repel each other depending on the intermolecular distance. At the conditions of Fig. 7, it is clear that the Lennard–Jones fluid is a good model for Krypton.

Fig. 8 shows the model performance for methane. The 173 K isotherm is subcritical. It has a vapor branch and a liquid branch. The vapor SDC values are from roughly 10 to 20 times greater than those of liquid methane. The model properly predicts such differences. The model also reproduces the shape of the 222 K isotherm which has a shape similar to that of a critical isotherm. At 454 K, the performance is also very good, for a true prediction, both, qualitatively and quantitatively. Notice that the pressure range in Fig. 8 is roughly from about 10 bar to about 2000 bar. Notice also that the model captures the rich variety of trends in Fig. 8 from the knowledge of only the real fluid experimental T_c, P_c and M_w. In spite of the non-spherical nature of methane molecules, the LJ fluid seems to be at good model

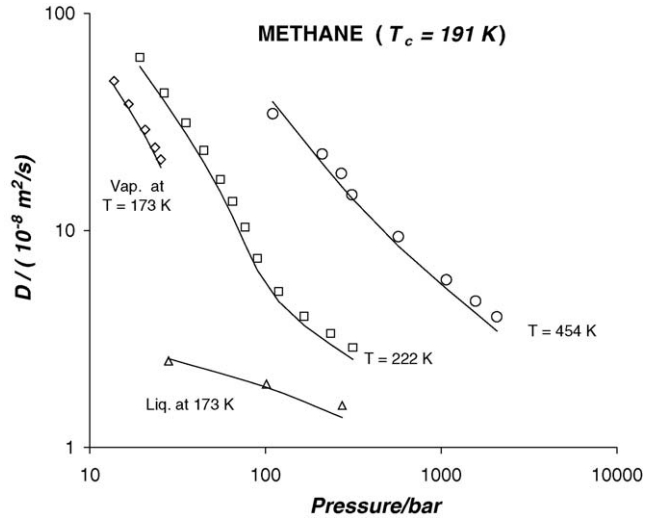

Fig. 8. Self-diffusion coefficient as a function of pressure for Methane, at varying temperature values. The solid lines correspond to model predictions. Experimental data: △ [32], ◊ [32], □ [32], ◯ [37].

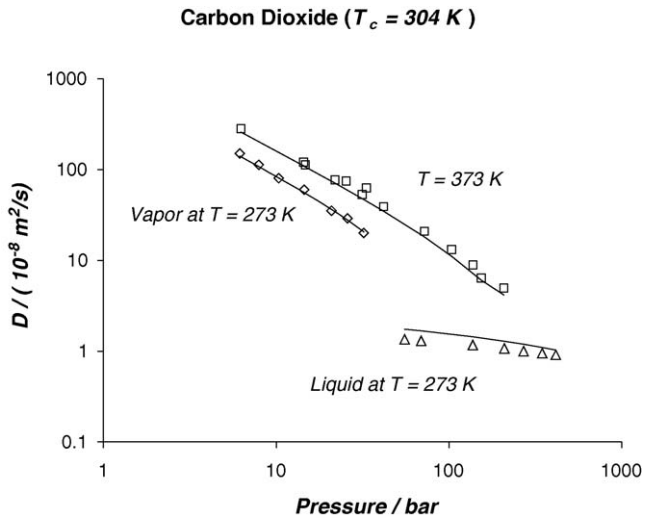

Fig. 9. Self-diffusion coefficient as a function of pressure for carbon dioxide, at varying temperature values. The solid lines correspond to model predictions. Experimental data: △ [29], ◊ [25] and [29], □ [25].

for methane, at least within the range of conditions of Fig. 8. The values for parameters ε and σ corresponding to Fig. 8 are those of Table 2, i.e., $\varepsilon/\kappa = 142.3$ K and $\sigma = 3.91$ Å. These are the values that one would use as input in a series of molecular simulation runs, performed for the range of conditions of Fig. 8. Such runs would match the solid lines of Fig. 8. When we perform a molecular simulation run, or use, equivalently, Eqs. (6) and (8), we acknowledge the existence of discrete molecules making up the fluid. In this sense, the parameters $\varepsilon/\kappa = 142.3$ K and $\sigma = 3.91$ Å are said here to be meaningful at molecular level for methane, in spite of the fact that the LJ functional form is one among several other forms that could be used to represent the effective interaction between methane molecules. Fully empirical correlations, on the other hand, can be obtained without assuming the fluid as constituted by molecules.

Fig. 9 compares, for vapor, liquid and supercritical-temperature carbon dioxide, model predictions and experimental data. The performance is good at the vapor and supercritical-temperature conditions. At liquid condition, we observe a relatively small systematic over prediction of the CO_2 self-diffusion coefficient. The pressure range in Fig. 9 is from a few bar to about 400 bar for liquid CO_2.

Fig. 10 presents the self-diffusion coefficient versus temperature for propane for four different isobars. The pressure, which is in the range from 250 to 2000 bar, is in all cases greater than the critical pressure of propane. The vertical dashed line is the boundary between the liquid state and the supercritical state. For the 500 and the 1000 bar isobars, the model performance is good. There is, however, some systematic model over prediction at 250 bar and a systematic under prediction at 2000 bar.

Fig. 11 shows the self-diffusion coefficient for perfluorocyclobutane as a function of pressure for three different isotherms. One of them is subcritical ($T = 373$ K) while the other two are supercritical ($T = 423$ and 473 K). The pressure range is from 50 to 1900 bar. In almost all cases we observe a systematic model over prediction of the self-diffusion coefficient. From the error

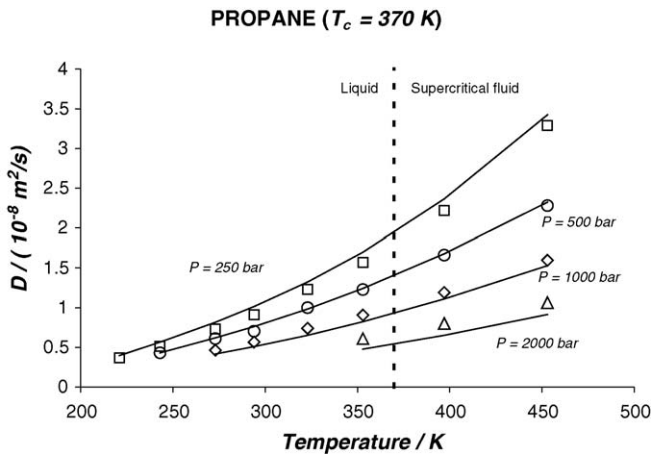

Fig. 10. Self-diffusion coefficient for propane as a function of temperature for varying pressure values. The solid lines correspond to model predictions. Symbols (△, ◊, ◯, □) denotes experimental data [37].

levels in Fig. 11, it is clear that forcing consistency between the LJ and real fluid critical point temperature and pressure values, is not enough to achieve an acceptable quantitative model performance for perfluorocyclobutane. In spite of the lack accuracy for this case, the model predicts the right trends that the SDC should follow as a function of temperature and pressure. This suggests that, to reduce the model errors, some additional parameter should be introduced for perfluorocyclobutane, which the user could fit against self-diffusion coefficient experimental data.

The previous figures illustrate, for a few real pure compounds, the performance of the present purely predictive Lennard–Jones-based model for the SDC. Table 3 provides quantitative model performance information for several fluids including those of the previous figures. The labels LIQ and VAP mean "liquid" and "vapor", respectively. The label light supercritical fluid (LSCF)

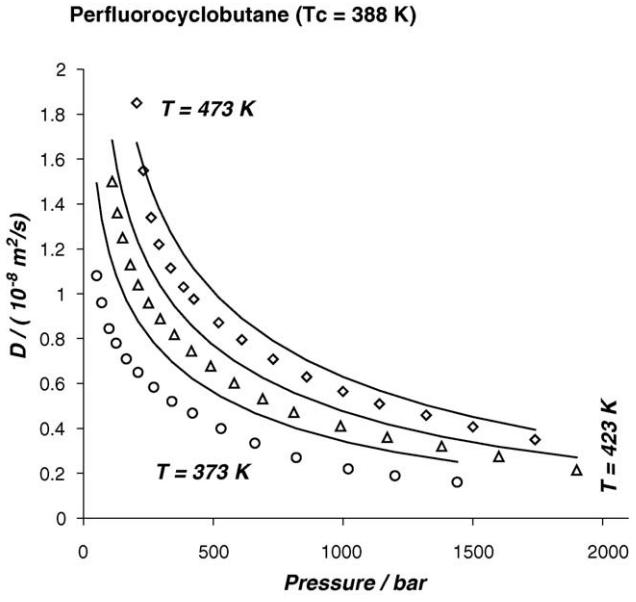

Fig. 11. Self-diffusion coefficient for perfluorocyclobutane as a function of pressure at varying temperature values. The solid lines correspond to model predictions. Symbols (◯, △, ◊) denotes experimental data [35].

implies that the fluid temperature is supercritical while the pressure is less than or equal to the critical pressure. In contrast, dense supercritical fluid (DSCF) implies a supercritical temperature and a pressure greater than the critical pressure. Our distinction between light and dense supercritical fluids is somewhat arbitrary but it helps to draw some general conclusions on the model behavior. The total number of data points considered in Table 3 is 1043. Silva et al. [43] used a larger database comprising 2471 data points. Our original database was of the same size than that of Ref. [43]. It shrunk, however, to a size of 1043 data points. The reasons for such shrinkage are: (a) part of the real fluid SDC experimental data corresponded to conditions falling outside the applicability ranges of Eqs. (6) and (8), and (b) another portion of the experimental data did not have the experimental pressure value reported. For cases where the density, rather than the pressure, was available, we could have estimated the pressure value using available methods to do so. Such an approach, however, would have introduced an additional source of uncertainty, i.e., the use of non-experimental input pressure information. We decided then to exclude from our analysis experimental points lacking pressure information. Our database, which is made of 1043 points, is still large enough to explore the potential of our modeling approach.

Table 3 shows, for every fluid and phase type (LIQ, VAP, LSCF or DSCF), the SDC average (AAD%) and maximum (Max AD%) absolute value percentage relative deviations associated to the present LJ-based model. Table 3 also reports the ranges of variation for temperature, pressure, reduced temperature T_r and reduced pressure P_r; and the number of experimental SDC data points together with the corresponding bibliographic sources.

Table 3 shows results for vapor (VAP) phases for carbon dioxide and methane. We see in both cases that the average prediction errors are less than or equal to 9% for both compounds, which is a good error level for a true prediction. The total number of VAP points is 46.

For light supercritical fluids we see that the average error is close to or less than 10% for krypton, methane, carbon tetrafluoride, chlorotrifluoromethane, carbon dioxide and ethylene. For the only LSCF water point the error is larger. Hence we see that, for LSCF fluids with relatively small non-polar or slightly polar molecules, the LJ-based predictions are quite acceptable in spite of the non-spherical nature of such real fluid molecules. The total number of LSCF points is 186.

For dense supercritical fluids, we find in Table 3 average errors less than or close to 10% for propane, methane, chloromethane, krypton and ethylene (total of 228 data points). Notice the high values for the maximum reduced pressure for most of these fluids. For water, the average error is 27%. Such large value might be due to the strong specific interactions existing among water molecules which Eq. (1) does not account for explicitly.

For liquids (310 points), we see average errors of at least 12%. Also notice the high values for the maximum practical reduced pressure for most of the LIQ fluids. For about seven out of the 18 LIQ fluids the prediction error level is quite acceptable (up to about 14%). For the remaining LIQ fluids, it is evident that the simple present LJ approach cannot describe the SDC

Table 3
Lennard–Jones-based prediction results of the self-diffusion coefficients of real fluids[a]

Compound	Phase type[b]	AAD%[c]	Max AD%[d]	No. of data points	Min T_r	Max T_r	Min P_r	Max P_r	Min T (K)	Max T (K)	Min P (bar)	Max P (bar)	References
Krypton	LIQ	21	28	3	0.88	0.95	1.74	1.8	184	200	96	99	[17]
Krypton	LSCF	6	17	49	1.05	1.40	0.10	1.0	219	293	6	53	[17,19,21]
Krypton	DSCF	10	21	27	1.00	1.31	1.04	2.0	210	274	57	113	[17,19]
Methane	VAP	9	14	11	0.81	0.98	0.21	0.8	155	187	10	37	[32]
Methane	LIQ	12	26	29	0.58	0.98	0.32	34.1	110	187	15	1568	[32,36]
Methane	LSCF	9	15	24	1.00	1.56	0.17	1.0	191	298	8	45	[32,34]
Methane	DSCF	8	20	151	1.00	2.38	1.06	45.0	191	454	49	2070	[32,34,37]
Ethane	LIQ	12	29	20	0.60	0.96	5.13	41.1	182	294	250	2000	[37]
Ethane	DSCF	14	25	20	1.04	1.49	5.13	41.1	319	454	250	2000	[37]
Propane	LIQ	13	33	26	0.60	0.97	0.35	47.1	221	359	15	2000	[27,37]
Propane	DSCF	8	19	10	1.07	1.22	5.89	47.1	397	453	250	2000	[37]
Cyclohexane	LIQ	93	146	17	0.57	0.69	0.02	19.6	313	383	1	800	[16]
Ethylene	LIQ	14	34	12	0.97	0.97	0.90	54.0	273	273	46	2722	[41]
Ethylene	LSCF	11	13	8	1.06	1.23	0.41	1.0	298	348	21	50	[40]
Ethylene	DSCF	12	26	36	1.06	1.23	1.01	36.3	298	348	51	1828	[40,41]
Benzene	LIQ	32	71	19	0.54	0.77	0.02	30.7	303	433	1	1505	[18,20]
Carbon dioxide	VAP	7	14	35	0.90	0.98	0.04	0.9	273	298	3	64	[25,26,29]
Carbon dioxide	LIQ	24	45	21	0.90	0.98	0.75	6.5	273	298	55	482	[27,29]
Carbon dioxide	LSCF	10	28	98	1.01	1.23	0.03	1.0	308	373	2	72	[25,26,29]
Carbon dioxide	DSCF	13	34	53	1.01	1.23	1.06	6.8	308	373	79	498	[25,26,29]
Chloromethane	LIQ	12	38	24	0.56	0.98	1.50	29.9	233	406	100	2000	[22]
Chloromethane	DSCF	10	22	4	1.06	1.06	7.49	29.9	440	440	500	2000	[22]
Dichloromethane	LIQ	18	33	13	0.53	0.80	1.64	32.9	270	406	100	2000	[22]
Chloroform	LIQ	22	42	30	0.55	0.74	0.02	27.4	295	397	1	1500	[22,24]
Trifluoromethane	LIQ	16	42	13	0.54	0.85	2.06	41.2	161	255	100	2000	[28]
Carbon tetrafluoride	LSCF	5	6	5	1.07	1.31	0.66	0.9	243	298	25	33	[30]
Carbon tetrafluoride	DSCF	29	101	49	1.07	1.53	1.04	12.0	243	348	39	450	[30]
Chlorotrifluoromethane	LIQ	13	33	22	0.60	0.97	6.46	51.7	180	294	250	2000	[33]
Chlorotrifluoromethane	LSCF	5	5	1	1.00	1.00	0.95	1.0	303	303	37	37	[31]
Chlorotrifluoromethane	DSCF	16	44	84	1.00	1.43	1.02	51.7	303	433	40	2000	[31,33]
Carbon disulphide	LIQ	22	33	5	0.54	0.57	0.01	5.8	298	313	1	457	[23]
Acetonitrile	LIQ	21	34	10	0.55	0.63	0.02	12.8	298	343	1	618	[39]
Tetramethylsilane	LIQ	51	94	12	0.66	0.83	1.60	35.5	298	373	45	1000	[18]
Perfluorocyclobutane	LIQ	55	93	23	0.83	0.96	1.80	51.8	323	373	50	1440	[35]
Perfluorocyclobutane	DSCF	14	26	34	1.09	1.22	3.96	68.4	423	473	110	1900	[35]
Pyridine	LIQ	13	26	11	0.54	0.68	0.02	17.8	333	423	1	1000	[38]
Water	LSCF	19	19	1	1.04	1.04	0.90	0.9	673	673	199	199	[15]
Water	DSCF	27	36	33	1.04	1.50	1.00	6.6	673	973	221	1459	[15]
Total				1043									

[a] Calculations performed according to Table 2 procedure.
[b] LIQ, liquid; VAP, vapor; LSCF, light supercritical fluid; DSCF, dense supercritical fluid.
[c] Average absolute-value percent relative deviation $= \mathrm{AAD\%} = \left(\frac{100}{\mathrm{NP}}\right) \sum_{i=1}^{\mathrm{NP}} \frac{|D_{\mathrm{pred}} - D_{\mathrm{exp}}|}{D_{\mathrm{exp}}}$.
[d] Maximum absolute-value percent relative deviation $= \mathrm{Max\ AD\%} = \max_{i=1}^{\mathrm{NP}} \left\{ \frac{100|D_{\mathrm{pred}} - D_{\mathrm{exp}}|}{D_{\mathrm{exp}}} \right\}$. NP = number of data points. D_{pred} = predicted self-diffusion coefficient. D_{exp} = experimental self-diffusion coefficient.

quantitatively. On the other hand, we have verified, for all the fluids in Table 3, that the model always gives the right trends for the SDC as a function of both, temperature and pressure. This fact suggests that the LJ fluid, with critical temperature and pressure values set equal to the real fluid values, could be used as a suitable reference for modeling the real fluid SDC, over a wide range of conditions, if proper corrections to account for non-sphericity and/or polarity are added, while using a general LJ PVT equation (Eq. (8)) for estimating the density.

The values of T_c and P_c, which we took from the DIPPR database [14], have variable uncertainty depending on the considered pure compound. Table 4 shows how the average error, AAD%, changes with ±2% changes in either T_c or P_c. Case A (C.A.) is the base case; it corresponds to the unperturbed original values of T_c and P_c in Ref. [14]. Hence, the AAD% values we report in column C.A. are the same than those in Table 3. We report them again in Table 4 to enable a quick comparison with the results for perturbed values of T_c and P_c. For instance, Case B (C.B.) corresponds to the unperturbed DIPPR value of T_c and to a value of P_c 2% lower than the DIPPR value. Notice that the number of data points under a given label, among the four possible, i.e., LIQ, VAP, LSCF or DSCF, may change when

Table 4
Sensitivity of the Lennard–Jones-based predicted self-diffusion coefficient with respect to the input critical pressure and critical temperature

Compound	Phase type	AAD%					Number of data points				
		C.A.	C.B.	C.C.	C.D.	C.E	C.A.	C.B.	C.C.	C.D.	C.E.
Krypton	LIQ	21	22	21	29	9	3	3	3	3	6
Krypton	LSCF	6	8	5	5	9	49	49	49	49	49
Krypton	DSCF	10	12	8	10	21	27	27	27	27	24
Methane	VAP	9	11	7	3	15	11	11	11	7	18
Methane	LIQ	12	12	12	10	17	29	29	29	27	32
Methane	LSCF	9	12	7	5	12	24	23	24	28	16
Methane	DSCF	8	9	7	6	12	151	152	151	153	149
Ethane	LIQ	12	12	11	10	15	20	20	20	20	20
Ethane	DSCF	14	15	14	11	17	20	20	20	20	20
Propane	LIQ	13	13	13	16	11	26	26	26	26	26
Propane	DSCF	8	8	8	8	9	10	10	10	10	10
Cyclohexane	LIQ	93	93	92	104	82	17	17	17	17	17
Ethylene	VAP	NA	NA	NA	220	NA	0	0	0	1	0
Ethylene	LIQ	14	14	14	14	16	12	12	12	11	12
Ethylene	LSCF	11	12	9	7	15	8	6	9	8	8
Ethylene	DSCF	12	14	10	8	20	36	38	35	36	36
Benzene	LIQ	32	33	32	39	27	19	19	19	19	19
Carbon dioxide	VAP	7	8	7	33	11	35	35	35	8	53
Carbon dioxide	LIQ	24	23	24	33	21	21	21	21	13	30
Carbon dioxide	LSCF	10	11	9	10	13	98	98	98	127	78
Carbon dioxide	DSCF	13	15	11	12	20	53	53	53	59	46
Chloromethane	LIQ	12	12	11	13	11	24	24	24	24	24
Chloromethane	DSCF	10	9	10	12	9	4	4	4	4	4
Dichloromethane	LIQ	18	18	17	20	16	13	13	13	13	13
Chloroform	LIQ	22	22	21	28	16	30	30	30	30	30
Trifluoromethane	LIQ	16	16	16	19	15	13	13	13	13	13
Carbon tetrafluoride	LSCF	5	3	7	10	2	5	5	5	5	5
Carbon tetrafluoride	DSCF	29	28	31	36	25	49	49	49	49	49
Chlorotrifluoromethane	LIQ	13	13	13	17	17	22	22	22	22	52
Chlorotrifluoromethane	LSCF	5	2	11	22	NA	1	1	1	1	0
Chlorotrifluoromethane	DSCF	16	15	22	36	10	84	84	84	84	55
Carbon disulphide	LIQ	22	21	22	17	26	5	5	5	5	5
Acetonitrile	LIQ	21	22	21	28	16	10	10	10	10	10
Tetramethylsilane	LIQ	51	51	51	57	44	12	12	12	12	12
Perfluorocyclobutane	LIQ	55	55	56	62	50	23	23	23	23	23
Perfluorocyclobutane	DSCF	14	13	15	18	11	34	34	34	34	34
Pyridine	LIQ	13	13	13	14	15	11	11	11	11	11
Water	LSCF	19	22	19	13	26	1	1	2	1	1
Water	DSCF	27	29	26	21	33	33	33	32	33	33
Total							1043	1043	1043	1043	1043

C.A.: $T_c = T_{c,DIPPR}$, $P_c = P_{c,DIPPR}$; C.B.: $T_c = T_{c,DIPPR}$, $P_c = 0.98P_{c,DIPPR}$; C.C.: $T_c = T_{c,DIPPR}$, $P_c = 1.02P_{c,DIPPR}$; C.D.: $T_c = 0.98T_{c,DIPPR}$, $P_c = P_{c,DIPPR}$; C.E.: $T_c = 1.02T_{c,DIPPR}$, $P_c = P_{c,DIPPR}$.

changing the values of T_c and/or P_c. From Table 4, we conclude that the calculated self-diffusion coefficient can be sensitive to the uncertainty in the input T_c and P_c values.

The results we showed for real fluids in Figs. 7–11, together with those of Table 3, make it possible to conclude that the modeling of SDC for real fluids based on SDC values for the LJ fluid, in wide ranges of conditions, for vapors, liquids and light and dense supercritical fluids, is in principle possible, without having to resort to (compound-specific or not) fully empirical pressure–density–temperature correlations. In other words, this work provides enough evidence of the suitability of using a PVT EOS of a model fluid (in this case the LJ fluid [Eq. (8)]) for estimating the volumetric properties of real fluids in the context of modeling self-diffusion coefficients.

We should stress that the data we used in this work are raw experimental data, i.e., we did not smooth them. This normally implies worse performance indices for analytical models such as the present one.

Table 3 should be seen as the result of the application of a corresponding states model where the reference fluid is the Lennard–Jones fluid. From Table 3, the present LJ-based corresponding states model has obvious limitations. Model fluids more realistic than the Lennard–Jones fluid could be tested as we did in this work. This requires, however, the availability, for the chosen model fluid, of values for thermodynamic and transport properties over a wide range of conditions, computed through typically long molecular simulation runs. In this work, we did not intend to model quantitatively the self-diffusion coefficient

behavior of complex real fluids, but to explore the potential of using the same reference model fluid for both, the PVT relationship and the SDC–temperature–density relationship.

8. Conclusions

In the present work we generated an analytical equation (Eq. (6)) for the Lennard–Jones self-diffusion coefficient as a function of temperature, density and LJ parameters ε and σ. We fitted Eq. (6) by imposing a good reproduction of recent high quality molecular simulation data [1,42] for the LJ fluid. Eq. (6) makes possible to avoid time-consuming molecular simulation runs when we need to compute a LJ SDC value. Using Eq. (6) and a pressure–density–temperature LJ equation of state [Eq. (8)] we generated a number of corresponding states charts (Figs. 1–6) for the SDC as function of temperature and pressure (or density). These charts are strictly valid for LJ fluids (two LJ fluids are different if their ε and σ parameters differ), but, at least at qualitative level, such charts agree well with those for pure real fluids. In this work, we treated real pure fluids as LJ fluids having a molecular weight (M_w), a critical temperature (T_c) and a critical pressure (P_c) identical to those of the real fluid. This choice makes it possible for the model to capture proper qualitative trends for the SDC in wide ranges of temperature and pressure. Using T_c, P_c and M_w as the only experimental input information, makes the model become a truly predictive one, i.e., we make no use of experimental real fluid SDCs for fitting the model. This has a cost, and implies that the model has a good quantitative performance if the considered real fluid is simple enough. For such simple enough fluids, it is remarkable the good behavior of the truly predictive model up to very high pressure values (see for instance Figs. 7–9).

Our main conclusion in this work is that it is suitable to base the modeling of the self-diffusion coefficient of real fluids, in wide ranges of temperature and pressure, on the SDC values measured for the LJ fluid (or better model fluids) through computer experiments, using a LJ pressure–density–temperature EOS rather than (compound-specific or not) empirical PVT correlations. For achieving a good quantitative performance for relatively complex fluids, corrections would be required which we did not intend to explore in this work. Another possibility would be to use a model fluid not limited to spherical molecules. The approach of incorporating corrections into the Lennard–Jones-based model could consist of making the intermolecular potential parameters ε and σ functions of additional characterization parameters and of the thermodynamic state through, e.g., the temperature [46]. This corresponds to the introduction of the so-called shape factors within the context of the extended corresponding states theory (ECST), as discussed by Ely and Hanley [47,48] and by Ely and Marrucho [46]. In this case, the result would be an ECS model where the reference fluid is a model fluid, i.e., the Lennard–Jones fluid, rather than a real fluid, as in usual ECS models. In real fluid-based ECS models, the correlations that describe the properties of the reference fluid interrelate macroscopic variables. On the other hand, in a model-fluid-based ECS model the analytical equations for the properties of the reference fluid would relate macroscopic variables to molecular level parameters. Available self-diffusion coefficient data sets are restricted to few real substances and cover only limited portions of the fluid region of the phase diagram [1], i.e., experimental real fluid self-diffusion coefficient data are not sufficiently comprehensive and accurate for any one fluid to serve as a satisfactory ECS reference fluid. This is one of the reasons for adopting a model fluid (e.g., LJ) rather than a real fluid as an ECS reference fluid. Additionally, while for real fluids it is difficult to measure the diffusion of a tagged particle that is of the same species than other particles in the fluid [1], self-diffusion coefficient values for model fluids can be determined with high accuracy in molecular dynamics simulations [1].

Notice that in this work we made a unified treatment of all possible fluid phase states: liquid, vapor and light and dense supercritical fluids.

Lennard–Jones theories have the ultimate goal of providing analytical expressions consistent with the available molecular simulation data for the LJ fluid. We should stress that the reader should see the results of Table 3 as the limit that the best LJ theories can reach under the restriction of full consistency with the experimental real fluid critical T, P coordinates. This is true due to the high accuracy levels that Eqs. (6) and (8) have within their ranges of applicability.

List of symbols

AAD%	average absolute value percent relative deviation
D	self-diffusion coefficient (SDC)
D_{exp}	experimental SDC
D_{pred}	predicted SDC
DSCF	dense supercritical fluid
EOS	equation of state
k	Boltzmann constant
LIQ	liquid
LJ	Lennard–Jones
LSCF	light supercritical fluid
m	mass of one molecule
Max AD%	maximum absolute value percent relative deviation
N	Number of molecules
N_A	Avogadro's number
NP	number of data points
P	absolute pressure
P_c	critical pressure
P_r	practical reduced pressure
PVT	pressure–volume–temperature
r	intermolecular distance
SDC	self-diffusion coefficient
SFE	solid–fluid equilibrium
T	absolute temperature
T_c	critical temperature
T_r	practical reduced temperature
u	potential energy
V	system volume
VAP	vapor
z	compressibility factor

Greek letters

ε	depth of the LJ potential well
$\rho^{+}_{\text{fluid,SFE}}$	dimensionless density of dense LJ fluid in equilibrium with LJ solid
ρ	Amount-of-substance density (in, e.g., mol cm^{-3} units)
ρ_c	critical amount-of-substance density (in, e.g., mol cm^{-3} units)
σ	LJ separation distance at zero energy

Acknowledgements

We are grateful to Elodie Gonon and Eliana Abreu for helping in the preparation of the digital self-diffusion coefficient database we used here; and, for financial support, to the European Commission (EVIDENT project, Contract No: JOF3-CT97-0034), to Consejo Nacional de Investigaciones Científicas y Técnicas de la República Argentina, and to University of Nevada, Reno.

Appendix A. Calculation of the limit of the product $(D^{+}\rho^{+})$ at zero density

To calculate $(D^{+}\rho^{+})_0$, i.e., the limit of the product $(D^{+}\rho^{+})$ as the density approaches zero, we used Eq. (B.1) of page 193 of Meier's [1] Ph.D. thesis, which rewritten in terms of dimensionless variables becomes the following:

$$(D^{+}\rho^{+})_0 = \frac{3}{8}\frac{f_{D\rho}}{\Omega^{(1,1)*}}\sqrt{\frac{T^{+}}{\pi}} \tag{A.1}$$

where the factor $(f_{D\rho}/\Omega^{(1,1)*})$ is defined by the following equations and by Table A.1. We replicate here, from Ref. [1], Eqs. (A.2)–(A.11) and Table A.1, for the sake of completeness:

$$f_{D\rho} = \frac{1}{(1-\Delta)} \tag{A.2}$$

$$\Delta = \frac{(6C^{*}-5)^2}{55-12B^{*}+16A^{*}} \tag{A.3}$$

$$A^{*} = \frac{\Omega^{(2,2)*}}{\Omega^{(1,1)*}} \tag{A.4}$$

$$B^{*} = \frac{5\Omega^{(1,2)*}-4\Omega^{(1,3)*}}{\Omega^{(1,1)*}} \tag{A.5}$$

$$C^{*} = \frac{\Omega^{(1,2)*}}{\Omega^{(1,1)*}} \tag{A.6}$$

Table A.1
Coefficients for Eqs. (A.7) and (A.8)

i	$a_i^{(1,1)*}$	$a_i^{(2,2)*}$
1	0.125431	0.310810
2	−0.167256	−0.171211
3	−0.265865	−0.715805
4	1.597600	2.486780
5	−1.190880	−1.783170
6	0.264833	0.394405

Values taken from Ref. [1], p. 196.

The quantities $\Omega^{(i,j)*}$ are the reduced collision integrals for the Lennard–Jones (12-6) intermolecular potential function of Eq. (1) of the text. The variables $\Omega^{(1,1)*}$ and $\Omega^{(2,2)*}$ are given, respectively, by the following equations:

$$\ln\,\Omega^{(1,1)*} = \left(-\frac{1}{6}\right)\ln(T^{+}) + \sum_{i=1}^{6} a_i^{(1,1)*}\times(T^{+})^{[(1-i)/2]} \tag{A.7}$$

$$\ln\,\Omega^{(2,2)*} = \left(-\frac{1}{6}\right)\ln(T^{+}) + \ln\left(\frac{17}{18}\right) + \sum_{i=1}^{6} a_i^{(2,2)*}\times(T^{+})^{[(1-i)/2]} \tag{A.8}$$

with coefficients $a_i^{(1,1)*}$ and $a_i^{(2,2)*}$ given in Table A.1.

The collision integrals $\Omega^{(1,2)*}$ and $\Omega^{(1,3)*}$ required in Eqs. (A.5) and (A.6) correspond to the following recurrence relation:

$$\Omega^{(i,j+1)*} = \Omega^{(i,j)*} + \frac{1}{j+2}T^{+}\frac{\partial\Omega^{(i,j)*}}{\partial T^{+}} \tag{A.9}$$

which gives for the particular cases of interest in the present work the following equations:

$$\Omega^{(1,2)*} = \Omega^{(1,1)*} + \frac{1}{3}T^{+}\frac{\partial\Omega^{(1,1)*}}{\partial T^{+}} \tag{A.10}$$

$$\Omega^{(1,3)*} = \Omega^{(1,2)*} + \frac{1}{4}T^{+}\frac{\partial\Omega^{(1,2)*}}{\partial T^{+}} \tag{A.11}$$

Eq. (A.1) has an extremely wide range of applicability: from $T^{+}=0.7$ to 1000.

References

[1] K. Meier, Computer Simulation and Interpretation of the Transport Coefficients of the Lennard–Jones Model Fluid, Shaker Verlag, Aachen, 2002, ISBN 3-8322-0968-9, pp. 12, 26, 220.
[2] R.C. Reid, J.M. Prausnitz, B.E. Poling, The Properties of Gases & Liquids, fourth ed., McGraw-Hill Internat, New York, 1987, pp. 392–393.
[3] H. Liu, E. Ruckenstein, Ind. Eng. Chem. Res. 36 (1997) 5488–5500.
[4] M.S. Zabaloy, J.M.V. Machado, E.A. Macedo, Int. J. Thermophys. 22 (2001) 829.
[5] E. Ruckenstein, H. Liu, Ind. Eng. Chem. Res. 36 (1997) 3927.
[6] Y. Zhu, X. Lu, J. Zhou, Y. Wang, J. Shi, Prediction of diffusion coefficients for gas, liquid and supercritical fluid: application to pure real fluids and infinite dilute binary solutions based on the simulation of Lennard–Jones fluid, Fluid Phase Equilib. 194–197 (2002) 1141–1159.
[7] R.L. Rowley, M.M. Painter, Int. J. Thermophys. 18 (1997) 1109.
[8] R. Agrawal, D.A. Kofke, Mol. Phys. 85 (1995) 43.
[9] H. Lee, G. Thodos, Ind. Eng. Chem. Fundam. 22 (1983) 17–26.
[10] S. De, Y. Shapir, E.H. Chimowitz, Chem. Eng. Sci. 56 (2001) 5003–5010.
[11] J. Kolafa, I. Nezbeda, Fluid Phase Equilib. 100 (1994) 1.
[12] R.B. Bird, W.E. Stewart, E.N. Lightfoot, Transport Phenomena, John Wiley & Sons, New York, 1960, p. 506.
[13] R.B. Bird, W.E. Stewart, E.N. Lightfoot, Transport Phenomena, second ed., John Wiley & Sons, New York, 2002, p. 522.
[14] DIPPR 801, Evaluated Process Design Data, Public Release (1998). American Institute of Chemical Engineers, Design Institute for Physical Property Data, BYU-DIPPR, Thermophysical Properties Laboratory. Provo, Utah.
[15] W.J. Lamb, G.A. Hoffman, J. Jonas, J. Chem. Phys. 74 (1981) 6875.

[16] J. Jonas, D. Hasha, S.G. Huang, J. Phys. Chem. 84 (1980) 109.
[17] P. Carelli, I. Modena, F.P. Ricci, Phys. Rev. A 7 (1973) 298.
[18] H.J. Parkhurst Jr., J. Jonas, J. Chem. Phys. 63 (1975) 2698.
[19] P. Carelli, A. De Santis, I. Modena, F.P. Ricci, Phys. Rev. A 13 (1976) 1131.
[20] A.F. Collins, L.A. Woolf, J. Chem. Soc. Faraday Trans. I 71 (1975) 2296.
[21] P. Codastefano, M.A. Ricci, V. Zaza, Physica 92A (1978) 315.
[22] F.X. Prielmeier, H.-D. Ludemann, Mol. Phys. 58 (1986) 593.
[23] L.A. Woolf, J. Chem. Soc., Faraday Trans. I 178 (1982) 583.
[24] K.R. Harris, H.N. Lam, E. Raedt, A.J. Easteal, W.E. Price, L.A. Woolf, Mol. Phys. 71 (1990) 1205.
[25] H. 0'Hern, J.J. Martin, Ind. Eng. Chem. 47 (1955) 2081.
[26] S. Takahashi, H. Iwasaki, Bull. Chem. Soc. Japan 39 (1996) 2105.
[27] R.C. Robinson, W.E. Stewart, Ind. Eng. Chem. Fundam. 7 (1968) 90.
[28] F.X. Prielmeier, E.W. Lang, H.-D. Ludemann, Mol. Phys. 52 (1984) 1105.
[29] P. Etesse, J.A. Zega, R. Kobayashi, J. Chem. Phys. 97 (1992) 2022.
[30] F. Khoury, R. Kobayashi, J. Chem. Phys. 55 (1971) 2439.
[31] K.R. Harris, Physica 93A (1978) 593.
[32] R. Dawson, F. Khoury, R. Kobayashi, A.I.Ch.E.J. 16 (1970) 725.
[33] M. Has, H.-D. Ludemann, Z. Naturf. 44a (1989) 1210.
[34] K.R. Harris, Physica 94A (1978) 448.
[35] R.J. Finney, M. Fury, J. Jonas, J. Chem. Phys. 66 (1977) 760.
[36] K.R. Harris, N.J. Trappeniers, Physica 104A (1980) 262.
[37] A.G. Schmid, S. Wappmann, M. Has, H.-D. Ludemann, J. Chem. Phys. 94 (1991) 5643.
[38] M. Fury, G. Munie, J. Jonas, J. Chem. Phys. 70 (1979) 1260.
[39] R.L. Hurle, L.A. Woolf, J. Chem. Soc. Faraday Trans. 178 (1982) 2233.
[40] S. Takahashi, J. Chem. Eng. Japan 10 (1977) 339.
[41] B. Arends, K.O. Prins, N.J. Trappeniers, Physica 107A (1981) 307.
[42] K. Meier, A. Laesecke, S. Kabelac, Int. J. Thermophys. 22 (2001) 161–173.
[43] C.M. Silva, H. Liu, E.A. Macedo, Chem. Eng. Sci. 53 (1998) 2423–2429.
[44] J.K. Johnson, J.A. Zollweg, K.E. Gubbins, Mol. Phys. 78 (1993) 591–618.
[45] J.J. Nicolas, K.E. Gubbins, W.W. Streett, D.J. Tildesley, Mol. Phys. 37 (1979) 1429–1454.
[46] J.F. Ely, I.M.F. Marrucho, The corresponding states principle, in: J.V. Sengers, R.R. Kayser, C.J. Peters, H.J. White Jr. (Eds.), Equations of State for Fluids and Fluid Mixtures. Part I, Elsevier, Amsterdam, 2000, pp. 291–292.
[47] J.F. Ely, H.J.M. Hanley, Ind. Eng. Chem. Fundam. (1981) 323–332.
[48] J.F. Ely, H.J.M. Hanley, Ind. Eng. Chem. Fundam. (1983) 90–97.